TECTONICS, VOL. 12, NO. 4, PAGES 911-924, AUGUST 1993

CRUSTAL STRUCTURE AND REFLECTIVITY OF THE SWISS ALPS FROM THREE-DIMENSIONAL SEISMIC MODELING 1. HELVETIC NAPPES

M. Stäuble[1] and O. A. Pfiffner
Geological Institute University of Bern, Bern, Switzerland,

S. B. Smithson
Department of Geology and Geophysics, University of Wyoming, Laramie

Abstract. Forward modeling based on combined geologic surface data, borehole and laboratory data on velocities, and seismic reflection data aid in understanding the seismic response in a transect through complex Alpine nappe structures. The synthetic seismic response from the model compares well with the observed data. The results suggest, however, that strong three-dimensional effects result in out-of-plane reflections and diffractions, as well as defocussing and scattering of seismic rays, thus rendering the use of two-dimensional migration techniques questionable. The model shows an unexpected rapid change in internal structure of the Helvetic nappes between the seismic line and outcrops located 6-8 km farther west. Moreover, the basement-cover interface on the northern flank of the Aar Massif, a basement uplift with a heave of 8 km, does not rise regularly in the hanging wall of a single major thrust fault, but rises in a series of steps due to several thrusts and folds. The northernmost structures appear to be fault-related open folds, whereas tight fold structures appear to dominate in the south.

[1]Also at Institute of Geophysics, ETH Zürich, Switzerland.

Paper number 93TC00378.
0278-7407/93/93TC00378$10.00

INTRODUCTION

In 1986, the Swiss National Research Program 20 (NFP 20) recorded approximately 120 km of multifold seismic data across the eastern Swiss Alps (Figure 1) with the aim of imaging structures observed at the surface which are likely to have a subsurface continuation and dip toward the seismic lines [Pfiffner et al. 1988, 1990a, b]. Because the plunging structures have been mapped in detail, these data can serve as calibration for crustal reflection surveys in a relatively young orogenic belt. One additional line, crossing the main NFP 20 profile at its northern end (Figure 2) was recorded in the mid-seventies by the Schweizerische Erdöl AG for exploration purposes and was reprocessed for this study by Stäuble.

Interpretation of the seismic data recorded in the Swiss Alps represents a three-dimensional problem because of the complex shape and plunge of the various tectonic units thrust northward over the Northalpine foreland. The tectonic style is characterized by fold-and-thrust structures, multifold imbrications, and considerable axial plunges attaining up to 30° (see also companion paper by Litak et al. [this issue]).

The purpose of this paper is to give a three-dimensional interpretation of the reflection profiles which cross the Helvetic nappes and its underlying units, using results from three-dimensional ray tracing and modeling software of SIERRA Geophysical Inc.

GEOLOGIC FRAMEWORK

The Helvetic Alps of eastern Switzerland have long been the aim of detailed studies. Here only a general outline of the geology is given; for detailed information, the reader is referred to Oberholzer [1933], Trümpy [1969], Schmid [1975], Pfiffner [1978, 1981, 1986], Funk et al. [1983], and Pfiffner et al. [1990a, b]. The study area (Figure 1) lies within the Helvetic zone and is south of the Molasse

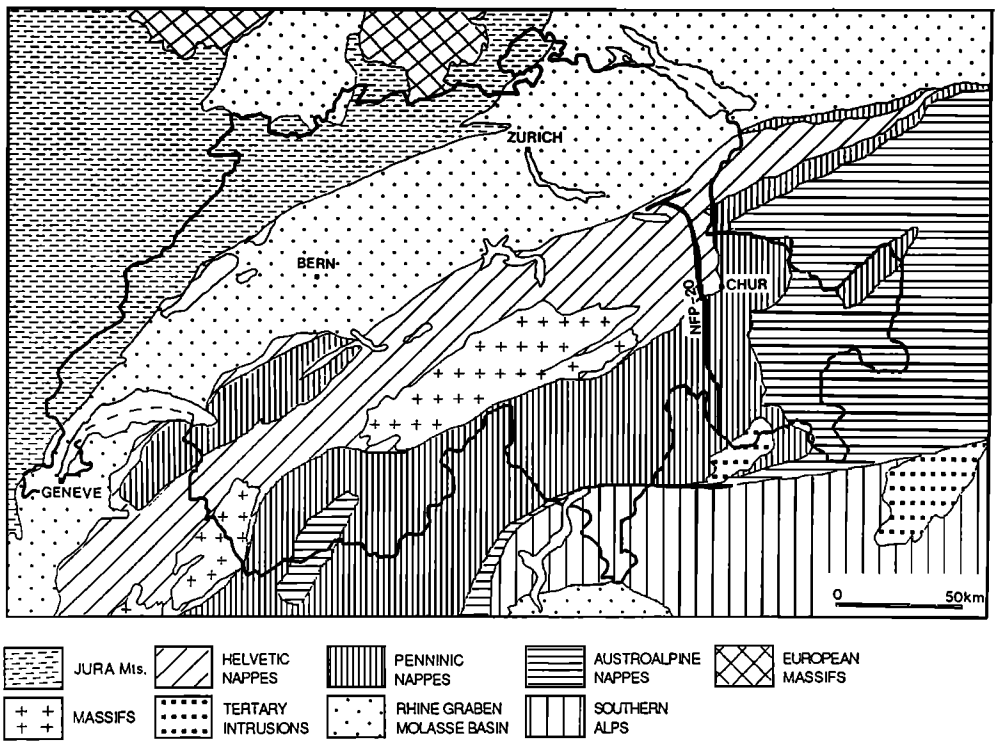

Fig. 1. Tectonic map of Switzerland showing the position of the seismic lines and the study area.

Basin. The major geological units covered are the Infrahelvetic complex, the Subalpine Molasse, and the Helvetic Nappes (Figure 2).

The Infrahelvetic complex [Milnes and Pfiffner, 1977] is the lowermost unit and consists essentially of crystalline basement rocks (including the Aar Massif basement uplift) and its Mesozoic to Oligocene cover sediments. The cover contains thick carbonate sequences (notably Triassic dolomites and Late Jurassic-Cretaceous limestones) interlayered with shaly and sandy clastics. The youngest sediments belong to an Eocene-Oligocene Flysch. The general structure of the Infrahelvetic complex comprises a combination of folding and thrusting at the interface between basement and cover rocks [Pfiffner et al. 1990a, b, and references therein]; thrust faults with considerable displacements and ductile folding at smaller scale are particularly conspicuous within the sedimentary cover [Pfiffner, 1978, 1985].

To the north the Subalpine Molasse consists of Oligocene to Miocene clastics which were imbricated and overridden by the Alpine nappes [see Stäuble and Pfiffner, 1991, and references therein]. These clastics were deposited in a peripheral foreland basin, the Molasse Basin, at the close of the Alpine collision. The study area covers the buried transition between the Flysch and Molasse sediments.

The Helvetic Nappes overly the Infrahelvetic complex to the south and the Subalpine Molasse to the north. In the cross section presented here, the Säntis thrust separates the Helvetic Nappes into two nappe complexes [Pfiffner, 1981]: the Lower Glarus nappe complex and the Upper Glarus nappe complex, which is also called Säntis Nappe. The Lower Glarus nappe complex consists of a series of imbricate thrust sheets in the northern part of the study area (Figure 3a). Toward the south this structural style gives way to folds (Figure 3b). The sedimentary rocks involved are of Triassic and Jurassic age with approximately 600 m of thick competent Upper Jurassic limestones forming the mechanically stiff layer. Secondary decoupling between these limestones and Triassic

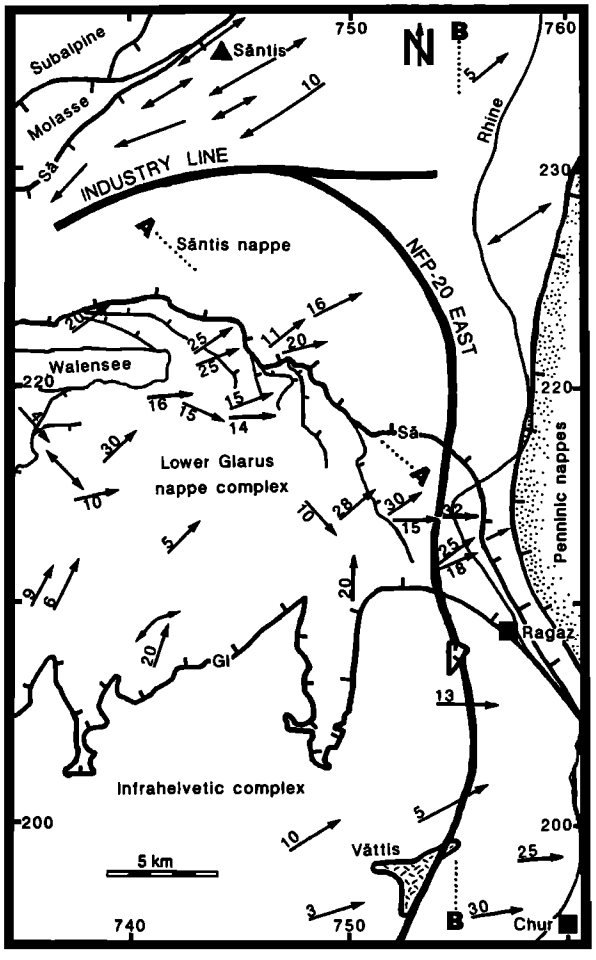

Fig. 2. Detailed geologic map and the location of the seismic lines. Key: Gl, Glarus; Sä, Säntis thrust; and AA and BB, traces of cross sections given in Figure 4. Arrows are major fold axes (with plunges)

dolomites occurs in the mechanically weak shales and sandstones of the Early and Middle Jurassic. The overlying Säntis Nappe consists of a folded, 1500-m-thick sequence of Cretaceous limestones (Figure 3a). They were detached from the underlying Jurassic limestones along the lowermost Cretaceous Palfris shales. This detachment, the Säntis thrust (Figure 3), produced a structural discontinuity between these two units. Particularly important for the seismic modeling is the 10°-30° east-northeasterly plunge of the fold axes in the Helvetic Nappes (Figure 2).

MODELING BASE

For the case studied here we have the rare possibility to observe structures at outcrop adjacent to the profile (Figure 3) which are very likely to continue into the seismic line and thus can be sampled by the seismic experiment.

The starting model is derived from previously published cross sections and maps, two of which are given in Figure 4. These cross sections are based on downdip projections and surface structural data and were completed by structure contour maps.

The determination of the velocity structure presented a serious problem because no borehole data are available in the Alps. Several different approaches were used to narrow down the possible range of velocities; they will now be discussed in more detail.

1. Borehole data from exploration wells drilled into the Molasse Basin northeast of the study area were used to determine the velocity of the Jurassic and the Tertiary sediments. Lithologies can be traced confidently over large distances, and studies by Lohr [1967, 1978] indicate a clear regional trend of velocities increasing from the Molasse Basin toward the Alps due to diagenetic lithification and increased overburden. For these reasons, the velocities given in Table 1 are considered to represent a lower limit of a possible range of seismic velocities.

2. Seismic velocities were measured in the laboratory from representative rock samples from the study area [Sellami et al., 1990]. Despite the influence of porosity, fluid content, pressure, temperature, and the high frequencies used, these velocities are considered to be more reliable than the values obtained from the other methods.

3. Interval velocities can be derived from stacking velocities, but care has to be applied in complex structures. Stacking velocities seem to increase toward the south. This trend, plus the average of the stacking velocities over the whole area, was used as an additional constraint.

Fig. 3 caption on page 915

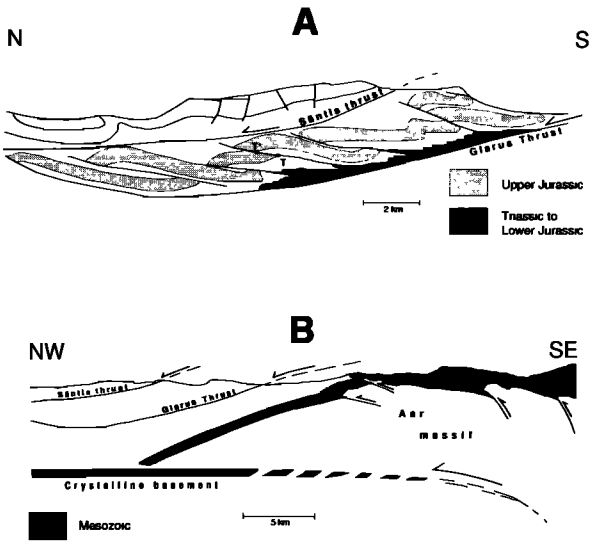

Fig. 4. Previously published geologic profiles form a basis for the starting model. Traces of profiles are given in Figure 2. (a) Structure of the Lower Glarus nappe complex; redrawn and completed from Trümpy [1969].
(b) Structure of the Infrahelvetic complex; redrawn from Pfiffner [1985].

4. A seismic refraction line was recorded in 1986 as part of the European Geotraverse EGT, which followed the NFP 20 profile. In 1987, as an accompanying experiment to the NFP 20, a refraction profile was recorded in the Helvetic zone along the northern Swiss Alps [Ye et al., 1990; Maurer, 1989]. Despite the limited resolution of these refraction profiles and the effects of anisotropy, the refraction data were included as an additional constraint on the velocity spectrum.

The values ultimately chosen for the modeling purpose are listed in the last column of Table 1. Whenever possible, they were picked from what is the most reliable method in the particular situation. The laboratory measurements, being nearly direct observations, are considered to be the best, the stacking velocities second.

Using the preferred velocities, the time sections were first transformed to depth. In a second step the reflections were correlated to lithologic contacts (cf. Pfiffner et al. [1990b] for details). In a third step the geologic interpretations of the two crossing seismic lines were combined with surface data. The resulting three-dimensional surfaces were contoured, digitized, and subsequently gridded into the model. This method could be used for the upper part of the model, the Helvetic Nappes with their prominent cross dip. For the lower part of the model cross dipping information was not available, and construction had to rely on velocity information and on extrapolation of surface data of the north dipping basement-cover contact (see Figure 4).

The complete model consists of 16 layers. Figure 5 shows two slices through the model. Within the Lower Glarus nappe complex reflections from the bottom of the imbricates are likely to stem from the base and the top of the Late Jurassic (Malm) limestones which are characterized by high seismic velocities of 5.9 km/s. The Glarus Thrust is not a visible reflection in the seismic section and is used here as a modeling tool only to define the base of the Lower Glarus nappe complex. The lowermost surface of the model is

Fig. 3. Structure of the Helvetic nappes along the transect of the NFP 20- EAST profile. The seismic line passes along the flank of the mountains behind the peaks visible in the photographs. Key: MJ, Middle Jurassic; UJ, Upper Jurassic; Cr, Cretaceous; and Sä, Säntis thrust. (a) The Upper Jurassic limestones beneath the Säntis thrust form an imbricate stack of thrust sheets. The thrust fault with offset T-T' is the same as given in the cross sections in Figures 4a and 10. The Cretaceous limestones above the Säntis thrust are folded. (b) The Upper Jurassic limestones show a transition from imbricate thrusting in the NNW to folding in the SSE. The Cretaceous limestones above the Säntis thrust are not affected by these structures.

TABLE 1. Velocities Derived From Several Different Methods

Lithologies	Approximate Depth, km	Well Data	Laboratory Data	Stacking Velocity	Refraction Data	Model Velocity
Säntis Nappe Cretaceous limestones	2.5	...	...	4.5-5.3	4.7-4.9	4.9
Lower Glarus nappe complex Malm limestones	2.5-4	...	6.05-6.64	5.4-6	4.7-4.8	5.9-6
Lower Glarus nappe complex Lias and Dogger (sandstones, shales)	4-4.5	...	...	4.8-5	...	4.8-5
Molasse and Flysch (sandstones, shales)	4.5-7.5	3.7-4.6	...	4.8-5	...	5.2
Infrahelvetic complex Malm limestones	7.5-8.5	5.3-6	6.2-6.41	5.4-5.8	5.7-5.8	6.2
Crystalline basement (granites, gneisses)	> 8.5	> 6	6.35-6.62	~ 6.2	5.8-6	6.3

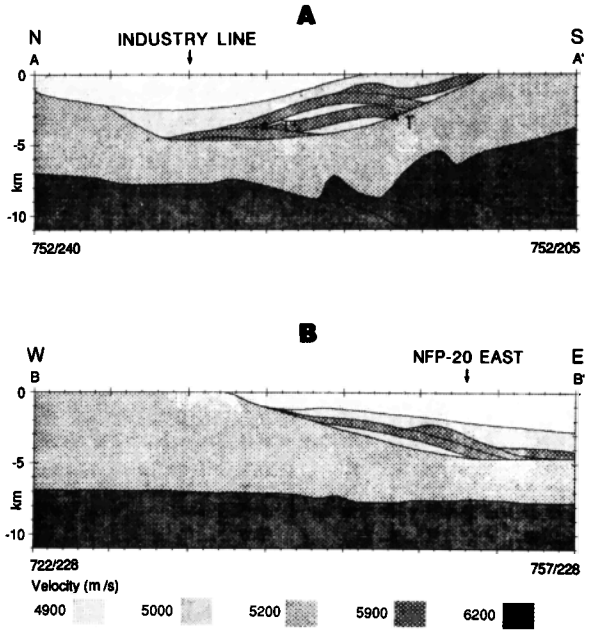

Fig. 5. Cross sections through the final model with the individual layers shaded according to the velocities. Traces of the cross sections are given in Figure 6.

the boundary between the Mesozoic carbonates and the overlying Tertiary Flysch (in the south) and Molasse (in the north). The basement-cover boundary is not modeled.

The display of an intelligible model in three dimensions proved to be a problem because the layers of the Lower Glarus nappe complex result in an obscure mixture of lines at this scale. For this reason the display of the model was primarily done in two-dimensional cross sections (Figure 5). In Figure 6a, the model is displayed in three dimensions, but stripped of the top layers (i.e., the Helvetic nappes) in order to fully show the shape of the lowermost layer, that is, the top of the Mesozoic.

FORWARD MODELING WITH RAY TRACING

Three-dimensional normal incidence ray tracing was used to test the validity of the model. The surface receiver arrays used for the ray tracing were those defined by the crooked line processing of the observed seismic lines NFP 20-EAST and the INDUSTRY line (Figure 2). The reflection coefficient series obtained from ray tracing were convolved with a zero-phase Ricker wavelet (a good approximation to mimic the stacked section) with a center frequency of 30 Hz as found in the data. The resulting synthetic sections were then compared with the field-recorded data. As an aid to determine from where the energy (i.e. the ray path) originates, two maps were plotted: (1) Contour maps of each layer with the depth points and the arrays (Figure 6b) and (2) three-dimensional models of the respective layers with the rays and the common-depth-point (CDP) line (Figure 6a).

Whenever discrepancies between model and observed seismic data necessitated changes, a new contour map was made, digitized, gridded, input into the model and tested again in the manner described above. Only the position and shape of the layers were changed, the velocities remained as originally defined as they are not well enough constrained. Starting at the top of the model, this process was repeated with each layer until a satisfactory match was achieved between the model response and the observed data. For this reason a complete starting model was never compiled, as every change in the top layer influenced the travel time of the rays. The starting model thus consisted of one layer. Only after a satisfactory match of the reflection from top layer and the observed data was achieved, was the next lower layer added to the model.

DISCUSSION AND CONCLUSIONS

Ray Tracing Results

A comparison between the observed sections and the synthetic sections is given in Figures 7 and 8. Although there is a close overall correspondence, a detailed comparison shows several minor discrepancies where position and shape of the synthetic reflector do not match perfectly with the observed data. Several limiting factors must be

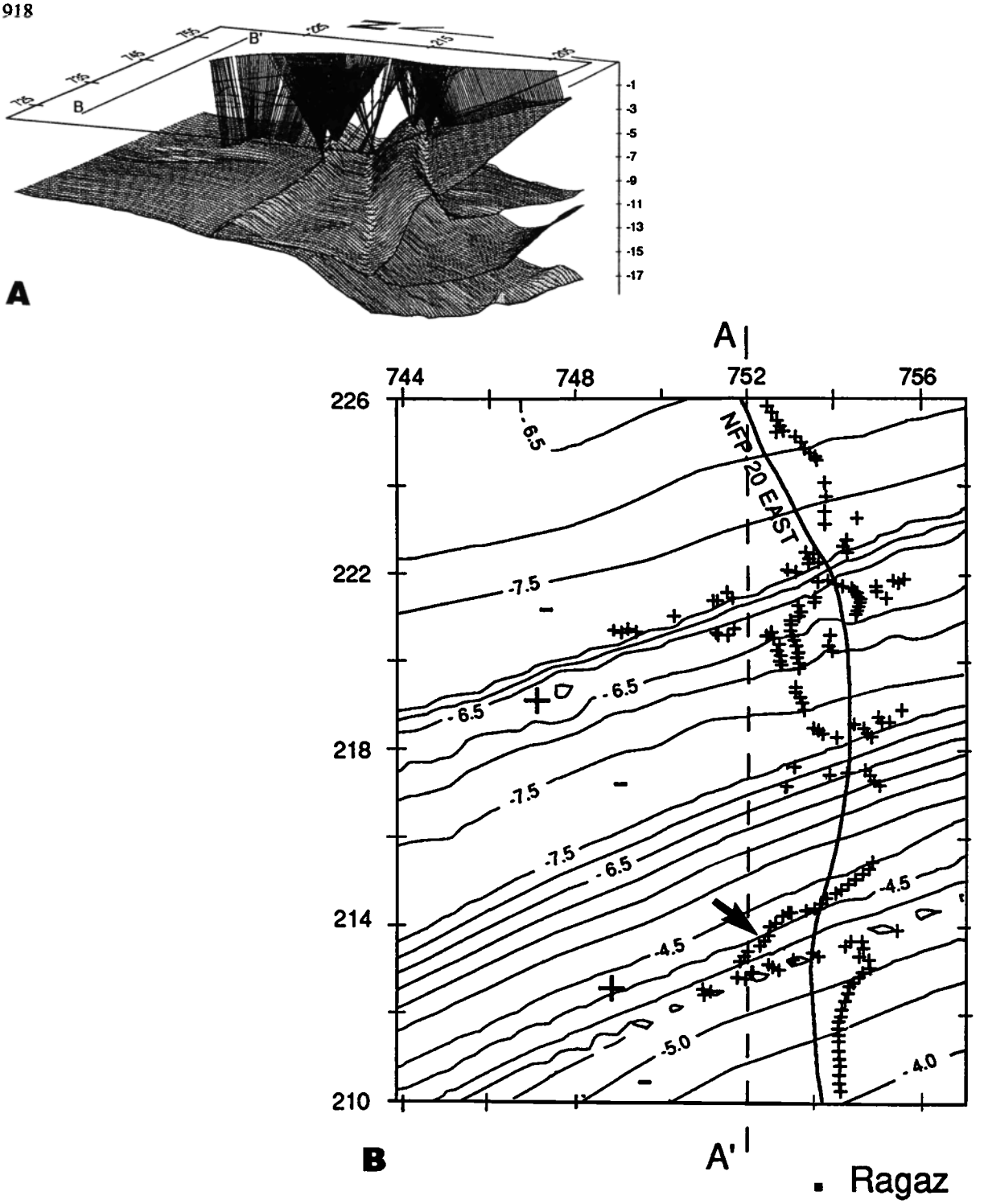

Fig. 6. (a) Three-dimensional display of the final model with the rays to the lowermost, that is, "Top Mesozoic" reflector. For better visibility the model is stripped of the top layers, that is, the Helvetic units. (b) Contour map of the same "Top Mesozoic" reflector with the ray endpoints (indicated by plus signs) showing the large scattering of the CDPs. Contours are in kilometers, structural highs and lows are indicated by (large) plus and minus signs. A-A' and B-B' are traces of the cross sections of Figure 5. Numbers show height in kilometers and Swiss national kilometer-grid system.

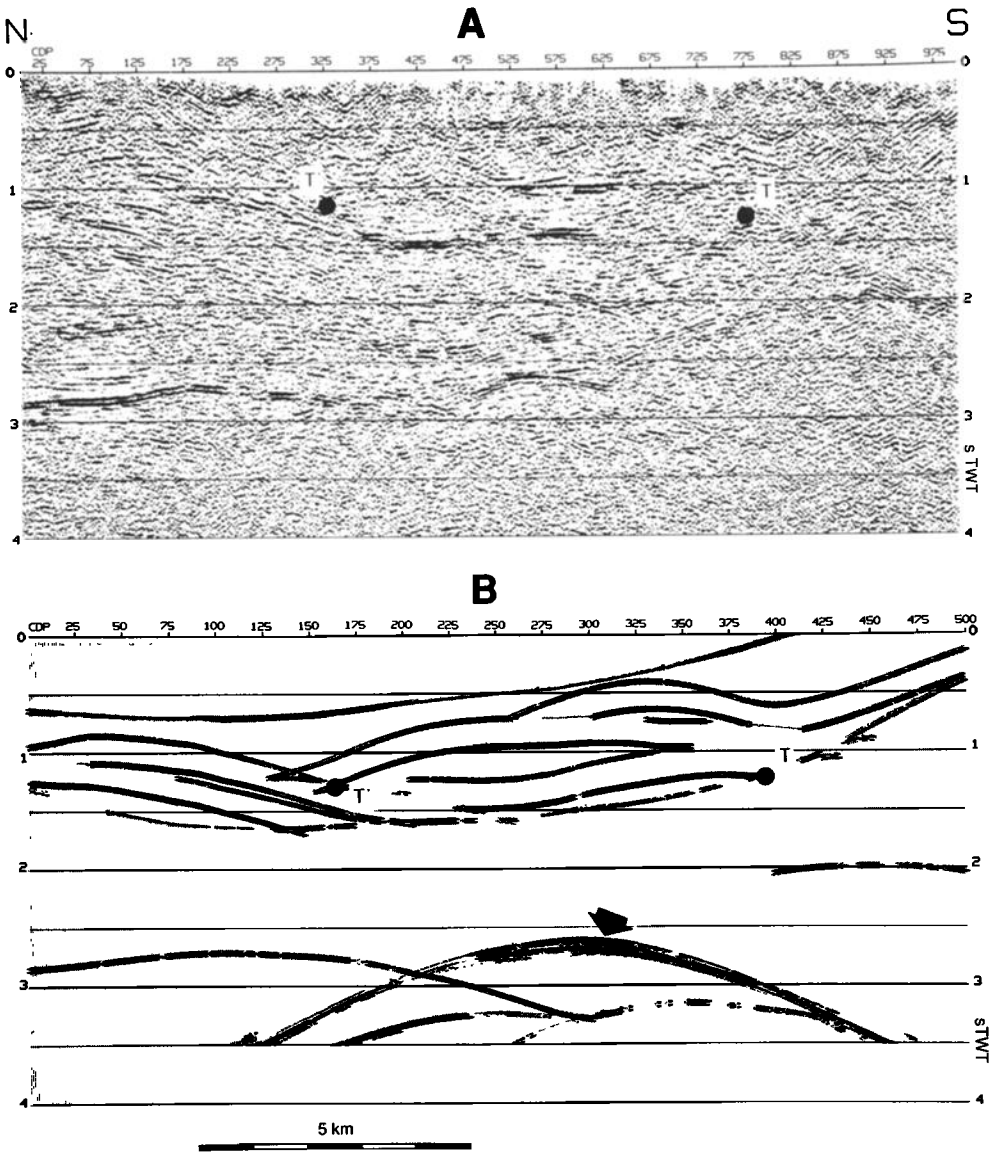

Fig. 7. (a) Unmigrated stack of seismic line NFP 20-EAST, (b) Synthetic seismogram of the NFP 20 profile using three-dimensional normal-incidence ray tracing.

taken into account to evaluate these mismatches:

1. The model only contains 16 layers, which is obviously a simplification of the real situation. In view of the particular geologic structure and the resolution of the seismic data, we consider this to be a sufficient approximation.

2. The velocity functions used in the model are approximations. Thus, for example, for a reflector at 1 s two-way time (TWT), modeled with a velocity of 5 km/s, a large error of +/-10% amounts to a variation in depth of the order of +/- 250 m.

3. With this uncertainty about the velocity, the dip of the contoured surfaces are approximations only, too. However, a change in dip would also result in sampling the layer at different positions. For instance, for a reflector outcropping 7 km laterally from the seismic section, a change in the depth by 100 m would result in a change in cross dip of 0.75° and an updip shift of the sampling point of 30 m.

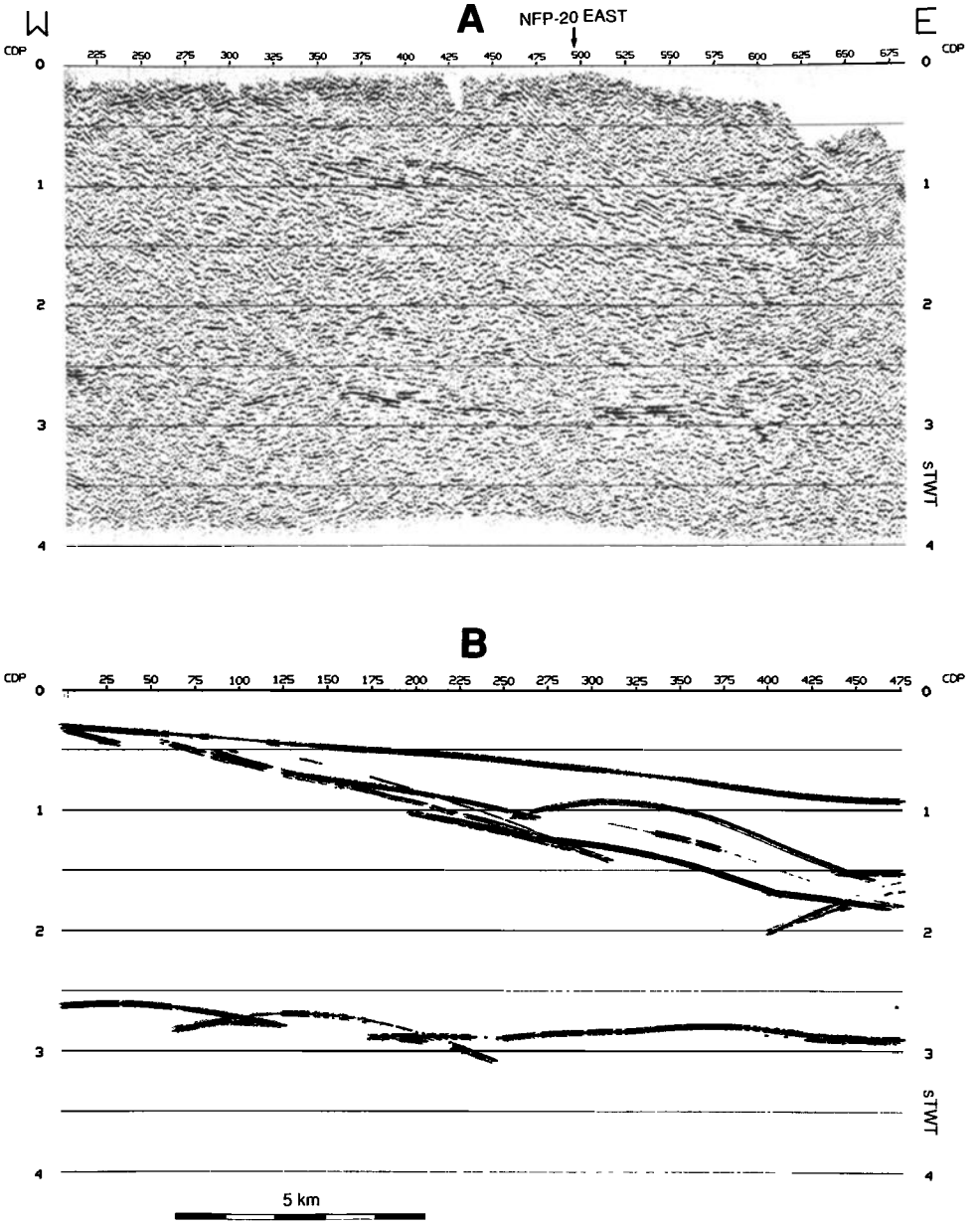

Fig. 8. (a) Unmigrated stack of E-W INDUSTRY line, b) Synthetic seismogram of the E-W profile using three-dimensional normal-incidence ray tracing.

4. When processing seismic data the one-dimensional assumption that a common-mid-point (CMP) is equal to a CDP is made. However, in a three-dimensional situation this assumption is not always fulfilled, and as a consequence, energy originating from a broad area is summed into a single CDP. This results in a considerable smearing (or loss in resolution) of the reflection. Incidentally, this "smearing" works in favor of the modeling technique, as small structural differences cannot always be modeled in detail. In Figure 6a the rays fan out of the two-dimensional plane, showing that the CMP=CDP assumption is not fulfilled. Moreover, normal-incidence ray tracing considers only rays with coincident shot and receiver points and therefore does not necessarily sample exactly the same areas as the field experiment.

Ray path analysis shows a strong three-dimensional effect resulting

in out-of-plane reflections and diffractions. The arcuate reflection between 2.5 and 3.5 s TWT in Figure 7b (indicated by an arrow) appears as a single strong event. Detailed analysis of the rays contributing to this reflection (arrow in Figure 6b), however, shows that it is a composite of several out-of-plane reflections.

Two-dimensional ray path analysis also suggests that defocussing effects from steep anticlines and diffractions from faults confuse the seismic image considerably [Stäuble and Pfiffner, 1991]. As an example a ray plot obtained from two-dimensional offset ray tracing is given in Figure 9 showing the extreme ray scattering and defocussing for shot point Ragaz.

In addition, recording of seismic data is often oblique to the geologic structures. Consequently, conventional migration techniques repositioning reflections in a two-dimensional plane, result in a wrong position for reflections like the ones discussed above and thus result in an erroneous interpretation. Furthermore, out-of-plane diffractions with a small curvature could be mistakenly treated as reflections. The three-dimensional ray tracing modeling technique used here yields good control of reflector geometry and avoids many of the problems inherent to two-dimensional migration.

Geologic Model

The geologic section corresponding to the three-dimensional final model with the best matching synthetic seismogram is shown in Figure 10. It shows all of the structures typical of the Alpine fold-and-thrust belt. The top two features of the model, the Säntis Nappe and the Säntis thrust appear as in any geologic profile. The imbricates within the Lower Glarus nappe complex are cut off in the model by the Glarus Thrust, which is due to modeling limitations of the SIERRA program. In reality the imbricate thrusts are

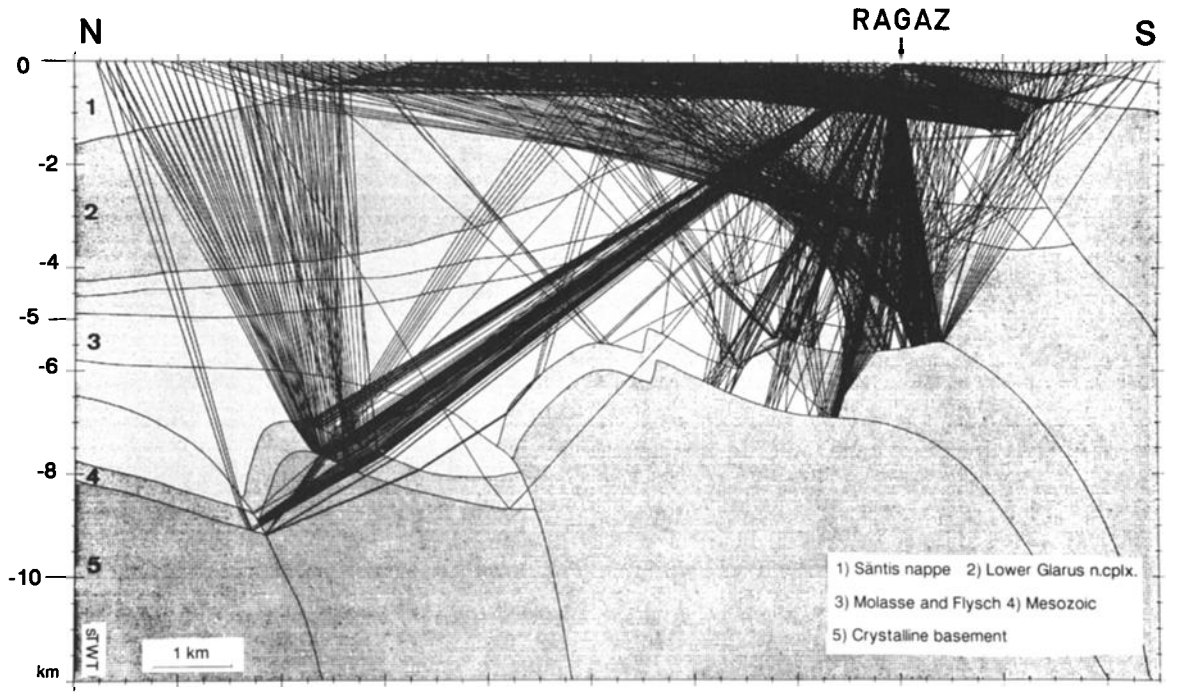

Fig. 9. Results from two-dimensional offset ray tracing on the northern flank of the Aar Massif (adapted from Stäuble and Pfiffner [1991]). The rays are shown from shotpoint RAGAZ (see Figure 2 for location) and show the importance of defocussing and scattering in this complex structural environment.

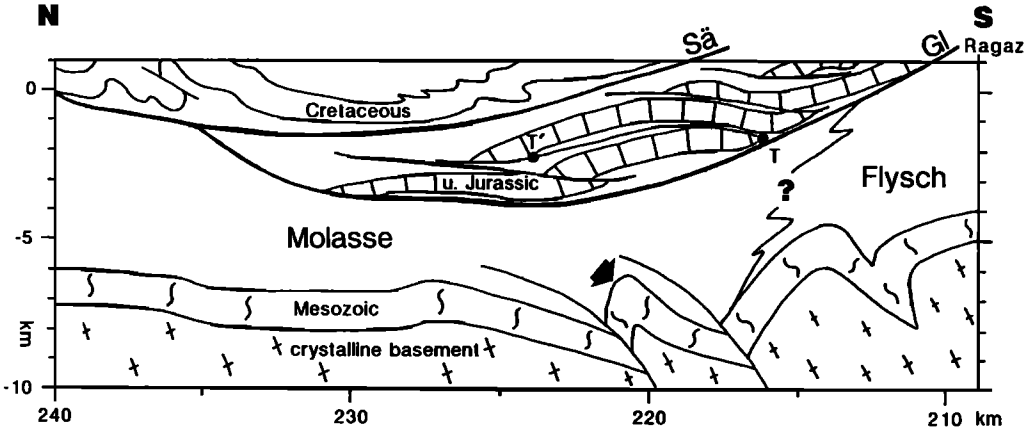

Fig. 10. Geologic interpretation of a N-S section from the three-dimensional model (Figure 5). The trace of the cross section is given in Figure 6. The seismic line covers the southern 2/3 of the cross section (S of km 230). The steep bulge of the Mesozoic (marked with an arrow) is interpreted as a compressional feature (ramp anticline). Note the large displacement (about 7.5 km) of the thrust fault marked T-T' (compared to less than 1 km in Figure 4a).

constrained to the Upper Jurassic limestones and do not extend all the way down to the Glarus Thrust [Pfiffner, 1981]. The following new geologic features emerge from this study.

The displacement along the Sennis thrust fault (marked T-T' in Figures. 3, 4a, and 10) increases from less than 1 km as observed at outcrop 5-7 km west of the study area, to 7-8 km as obtained from modeling. Comparing the initial and final geologic profiles (Figures 4a and 10), it follows that the internal structure of the imbricate thrust sheets within the Lower Glarus nappe complex changes going east. In particular, an increase in nappe internal shortening by more extensive imbrications results in a greater thickness of the whole Lower Glarus nappe complex. Since the upper bound of this nappe complex (the Säntis thrust) is well constrained, it must be assumed that its lower bound, the Glarus Thrust, must be located at a depth of -3.5 km rather than at -2.5 km as assumed in the initial model. This result, derived from three-dimensional seismic modeling, places serious constraints on downdip projections over even moderate distances in the Helvetic Nappes.

The increase in shortening in the footwall of the Säntis thrust also points to a decrease in displacement along the Säntis thrust. Such a change was expected but further eastward. East of the Rhine river the Upper Jurassic and Cretaceous limestones are folded more or less harmonically without any sign of thrust separation between the two units. The results obtained from this modeling suggest that the displacement along the Säntis thrust vanishes laterally much sooner than anticipated.

The basement-cover contact on the northern flank of the Aar Massif is at a depth of about -7.5 km beneath the central part of the study area. It then rises southward in a series of steps due to thrusting and folding and is exposed in the Vättis inlier situated 5 km south of the section discussed here (Figure 2). In the model the northernmost of these steps appears as a ramp anticline (marked with an arrow in Figure 10), which was unexpected from the seismic field data or from geological observations.

A basal thrust as shown in Figure 4b, putting basement onto a slab of Mesozoic cover rocks, has been proposed for this transect [Pfiffner, 1985] as well as for a transect through the Western Alps [Guellec et al., 1990; Butler 1986] If present, such a slab of Mesozoic would have been recorded. If, on the other

hand, as suggested by Guellec et al. [1990] for the Western Alps, a low-angle thrust fault putting basement onto basement is postulated, this contact would likely be associated with a mylonite zone. The absence of reflections in the NFP0 20-EAST profile can be explained in several ways: (1) There is no such thrust fault; (2) the thrust fault is associated with a very thin mylonite zone (beyond the resolution of the seismic experiment) and therefore possibly being of little importance (i.e., having a small displacement only); or (3) the thrust fault and the associated mylonite zone dip steeply (and therefore not imaged seismically) and the displacement is relatively small.

In the geologic interpretation (Figure 10) the last possibility is retained. This structural style is in fact observed at the surface some 50 km farther west [Pfiffner et al. 1990a].

Acknowledgments. The work was funded by the Swiss National Research Program NFP 20. P. Valasek provided valuable help as well as critically reading the manuscript. We thank S. Müller for continuous support. The paper benefitted greatly by critical review of L. Brown and D. Snyder. We are grateful to the BEB, Hannover (D) and the Swisspetrol Holding AG for the industry line granted in exchange with the NFP 20 data. Thanks are extended to A. Werthemann, I. Blaser, and W. Schaad for technical assistance.

REFERENCES

Butler, R.W.H., Thrust tectonics, deep structure and crustal subduction in the Alps and the Himalayas, *J. Geol. Soc. London, 143,* 857-873, 1986.

Funk, H.P., T. Labhart, A.G. Milnes, O.A. Pfiffner, U. Schaltegger, C. Schindler, S.M. Schmid, and R. Trümpy, Bericht über die Jubiläumsexkursion "Mechanismus der Gebirgsbildung" der Schweizerischen Geologischen Gesellschaft in das ost- und zentralschweizerische Helvetikum, *Eclogae Geol. Helv., 76,* 91-123, 1983.

Guellec, S., J.L. Mugnier, M. Tardy, and F. Roure, Neogene evolution of the western Alpine foreland in the light of ECORS data and balanced cross sections, in *Deep Structure of the Alps,* edited by F. Roure, P. Heitzmann, and R. Polino, Mém. Soc. Géol. Fr., 156, 165-184, 1990.

Litak, R.K., R.H. Marchant, O.A. Pfiffner, L.D. Brown, S. Sellami, L. Levato, J.-J. Wagner, and R. Olivier, Crustal structure and reflectivity of the Swiss Alps, from three-dimensional seismic modeling: 2. Penninic nappes, *Tectonics,* this issue.

Lohr, J., Die seismischen Geschwindigkeiten in der Ostschweiz, *Bull. Ver. Schweiz. Petrol. Geol. u. Ing., 34,* 29-38, 1967.

Lohr J., Alpine Stress Documented by Anomalous Seismic Velocities in the Molasse Trough, in *Alps, Apennines, Hellenides, Geodynamic Investigations along Geotraverses,* edited by H. Closs, D. Roeder, and K. Schmidt, E. Schweizerbart Vlg., Stuttgart, 1978.

Maurer, H., Die Struktur der Erdkruste unter dem schweizerischen Alpennordrand, Diploma thesis, *Eidg. Techn. Hochschule Zürich,* Switzerland, 1989.

Milnes A.G., and O.A. Pfiffner, Structural development of the Infrahelvetic complex, eastern Switzerland, *Eclog. Geol. Helv., 70,* 83-95, 1977.

Oberholzer, J., Geologie der Glarner Alpen, *Beitr. Geol. Karte Schweiz, n.F. 28,* 1-626 and Atlas,1933.

Pfiffner, O.A., Der Falten und Kleindeckenbau im Infrahelvetikum der Ostschweiz, *Eclog. Geol. Helv., 71,* 61-84, 1978.

Pfiffner, O.A., Fold-and-thrust tectonics in the Helvetic Nappes (E. Switzerland), in *Thrust and Nappe Tectonics,* edited by K. R. McClay, and N.J. Price, *Spec. Publ. geol. Soc. London,9,* 319-327, 1981.

Pfiffner, O.A., Displacement along thrust faults, *Eclog. Geol. Helv., 78,* 313-333, 1985.

Pfiffner, O.A., Evolution of the north Alpine foreland basin in the Central Alps, in *Foreland basins,* edited by P.A. Allen, and P. Homewood, *Spec. Pub. Int. Assoc. Sedimentol., 8,* 219-228, 1986.

Pfiffner, O.A., W. Frei, P. Finckh, and P. Valasek, Deep seismic reflection profiling in the Swiss Alps: Explosion seismology results for line NFP 20-EAST, *Geology, 16,* 987-990, 1988.

Pfiffner, O.A., E.M Klaper, A.-M. Mayerat, and P. Heitzmann, Structure of the basement-cover-contact in the Swiss Alps, in *Deep Structure of the Alps,* edited by F. Roure, P. Heitzmann, and R. Polino, Mém. Soc. Géol. Fr., 156, 247-262, 1990a.

Pfiffner, O.A., W. Frei, P. Valasek, M. Stäuble, L. Levato, L. DuBois, S.M. Schmid, and S.B. Smithson, Crustal shortening in the Alpine Orogen: Results from deep seismic reflection profiling in the eastern Swiss Alps, Line NFP 20-EAST, *Tectonics, 9,* 1327-1355, 1990b.

Schmid, S.M., The Glarus Thrust: Field evidence and mechanical model, *Eclog. Geol. Helv., 68,* 247-280, 1975.

Sellami, S., F. Barblan, A.-M. Mayerat, O.A. Pfiffner, K. Risnes, and J.-J. Wagner, Compressional wave velocities of samples from the NFP 20-EAST profile, in *Deep Structure of the Alps,* edited by F. Roure, P. Heitzmann, and R. Polino, Mém. Soc. Géol. Fr., 156, 77-84, 1990.

Stäuble, M., and O.A. Pfiffner, Evaluation of the seismic response of basement fold-and-thrust geometry in the Central Alps based on 2-D ray tracing, *Ann. Tectonicae, V/1,* 3-17, 1991.

Trümpy, R., Die Helvetischen Decken der Ostschweiz. Versuch einer palinspastischen Korrelation und Ansätze zu einer kinematischen Analyse, *Eclog. Geol. Helv., 62,* 105-142, 1969.

Ye, S., and J. Ansorge, A crustal section through the Alps derived from EGT seismic refraction data, in *The European Geotraverse: Integrative studies,* edited by R. Freeman, P. Giese, and S. Mueller, pp. 221-236, European Science Foundation, Strasbourg, Fr., 1990.

O.A. Pfiffner, Geological Institute, Baltzerstr. 1, CH-3012 Bern, Switzerland.

S.B. Smithson, Department of Geology and Geophysics, University of Wyoming, Laramie, WY 82071.

M. Stäuble, KSEPL, Shell Research, Postbus 60, 2280 AB Rijswijk, Holland.

(Received March 19, 1991; revised May 15, 1991; accepted February 11, 1993.)